Misfit relaxation of the AlN/Al_2O_3 (0001) interface

Th. Kehagias,[1] Ph. Komninou,[1,*] G. Nouet,[2] P. Ruterana,[2] and Th. Karakostas[1]
[1]*Physics Department, Aristotle University of Thessaloniki, 540 06 Thessaloniki, Greece*
[2]*ESCTM-CRISMAT, UMR 6508 CNRS, ISMRA, 6 Boul. Marechal Juin, 14050 Caen Cedex, France*
(Received 16 November 2000; revised manuscript received 15 June 2001; published 29 October 2001)

The epitaxial interface formed by a thin buffer layer of AlN deposited by molecular beam epitaxy on (0001) Al_2O_3 is investigated using electron microscopy techniques. Plan-view observations display a two-dimensional translational moiré pattern resulting from the difference in lattice parameters between the two crystals. The effective misfit of -0.1091 suggests the presence of a network of 60° misfit interfacial dislocations. These are, most of the time, introduced every 8 atomic planes of the AlN lattice or 9 atomic planes of the Al_2O_3 lattice, which is directly verified by cross-section high-resolution electron microscopy (HREM). The density of threading dislocations terminating at the buffer/substrate interface is in agreement with the density of threading dislocations near the surface of the GaN film. This in conjunction with terminating fringes observed in the moiré patterns provides strong evidence that threading dislocations are connected with the interfacial misfit dislocations. Plan-view HREM images reveal that a threading dislocation is directly related to two extra prismatic AlN half-planes, the missing parts of which are associated with two misfit dislocations in the interfacial network. The Burgers vector of the threading dislocation equals the sum of the Burgers vectors of the two misfit dislocations and therefore is of the **a** type. Although misfit dislocations relax the larger fraction of the misfit strain, the AlN buffer layer is still under a compressive residual strain (-8.2×10^{-3}), since the effective misfit is smaller than the natural misfit between the two lattices.

DOI: 10.1103/PhysRevB.64.195329 PACS number(s): 81.05.Ea, 68.37.Lp, 61.72.Ff, 68.55.Ac

I. INTRODUCTION

The growth of GaN films, an important new material for microelectronic applications, is extensively investigated using various deposition techniques and substrates. For the epitaxial growth of active GaN layers, the AlN/Al_2O_3 or GaN/Al_2O_3 heterophase systems in (0001) orientation are widely used as buffer/substrate systems. The study of misfit relaxation in the AlN/Al_2O_3 and GaN/Al_2O_3 systems is very important, since most of the defective structures present in the GaN films originate from the buffer/substrate interface. These defects are responsible for the low efficiency of the devices and should be studied extensively.[1] The mechanisms leading to the nucleation of misfit dislocations in strained epitaxial layered structures has been an important matter of study of interfacial relaxation.[2] In the GaN/Al_2O_3 system the misfit is partially relaxed by dislocations confined at the interface.[3] Moreover, Kaiser *et al.* argued that residual elastic strain causes a density of 10^{10} cm^{-2} threading dislocations in the GaN overgrowth. Investigation of the interface of layered heterostructures in plan-view orientation is important since it gives direct images of the in-plane interfacial defects and provides valuable information about the structure of the out-of-plane defects in the initial stages of growth. For instance, the bending of threading dislocations into the buffer/substrate interfacial plane may be indicated by terminating moiré fringes.[4]

In this paper, we analyze the structural defects that are introduced in the AlN/Al_2O_3 interface due to the mismatch between the two crystal lattices, using transmission and high-resolution electron microscopy in both plan-view and cross-section geometry. In particular, the compressive strain exerted on the AlN epilayer, which is accommodated by a 60° misfit dislocation network and a residual elastic strain, is calculated in terms of moiré fringe patterns. The correlation between misfit and threading dislocations is directly revealed in high-resolution electron microscopy (HREM) images and verified by comparing dislocation densities at the buffer/substrate interface and near the GaN overgrowth surface. Finally, a Burgers circuit around the core of a threading dislocation emerging from the epitaxial AlN/Al_2O_3 interface is presented and the relevance of the determined Burgers vector with the Burgers vectors of the associated misfit dislocations is shown.

II. EXPERIMENTAL METHODS

Molecular beam epitaxy (MBE) was used for the deposition of the AlN buffer on Al_2O_3, at 800 °C, until a thickness of 100 nm was reached. On the top of the buffer layer a 1-μm Mg-doped GaN overgrowth was deposited. Samples for plan-view and cross-section electron microscopy (XTEM) were prepared using first the standard technique of mechanical thinning down to 30 μm specimen thickness, followed by appropriate ion milling. Plan-view specimens, in particular, were ion milled not only from the substrate side, but also from the GaN film side and under continuous monitoring the desired AlN/Al_2O_3 interface was revealed. Transmission electron microscopy (TEM) observations were carried out in the Jeol JEM 120 CX electron microscope operated at 120 kV and HREM observations in a Topcon 002 B electron microscope operated at 200 kV, with a point to point resolution of 0.18 nm and $C_s = 0.4$ mm. All TEM experimental values bare a precision of $\pm 1\%$.

 ©2001 The American Physical Society

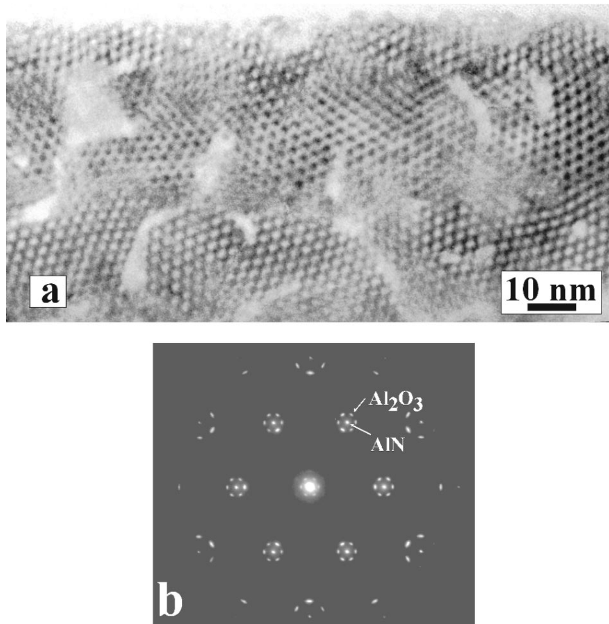

FIG. 1. (a) Plan-view bright-field (BF) HREM micrograph illustrating a two-dimensional translational moiré pattern due to overlapping of the AlN epilayer and the Al_2O_3 substrate in (0001) orientation. The micrograph reveals the hexagonal symmetry of the heterophase interface and the coalescence of adjacent AlN islands during the initial stages of growth. (b) The corresponding common diffraction pattern; satellite spots around basic reflections arise due to double diffraction.

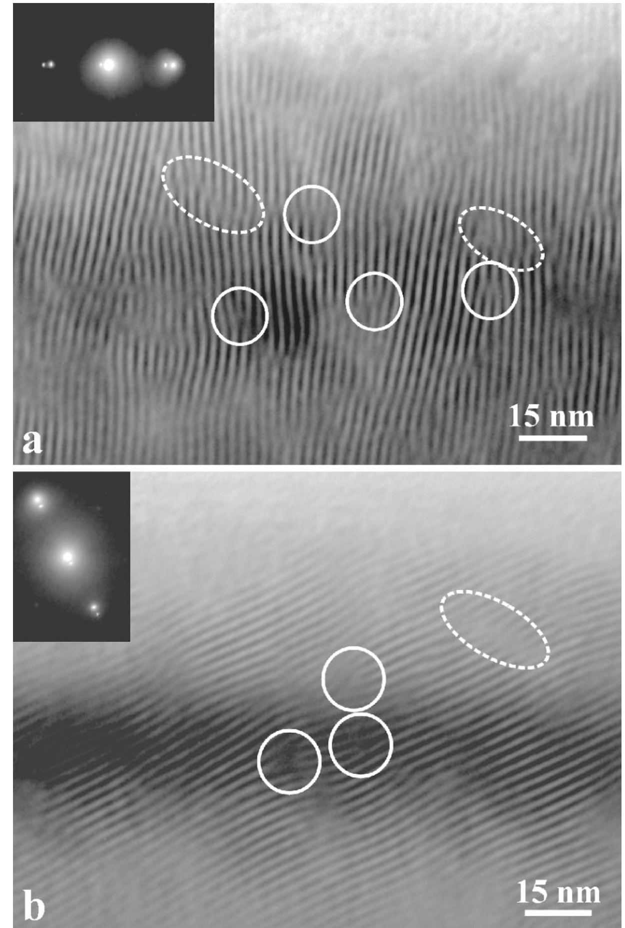

FIG. 2. (a) Plan-view BF TEM micrograph showing a fringe translational moiré pattern, when only one set of $10\bar{1}0/11\bar{2}0$ reflections of the AlN/Al_2O_3 system is operated, respectively. (b) A second fringe moiré pattern appears when a different set of equivalent reflections of the AlN/Al_2O_3 system is operated. The presence of out-of-plane line and planar defects, crossing the epilayer, is revealed either by terminating moiré fringes (threading dislocations) or by discontinuous shifts of moiré fringes (SF's). The edge component of threading dislocations is visualized inside solid circles, whereas traces of SF's are included inside dashed ellipses. Corresponding diffraction patterns are shown as inserts.

III. RESULTS

In the AlN/Al_2O_3 heterophase system the epitaxial relationship between the two crystal lattices is $(0001)AlN//(0001)Al_2O_3$ and $\langle 10\bar{1}0\rangle AlN//\langle 11\bar{2}0\rangle Al_2O_3$. Thus, the $\{10\bar{1}0\}$ planes of the AlN epilayer are oriented exactly parallel to the $\{11\bar{2}0\}$ planes of the Al_2O_3 substrate. During observation of the plan-view samples, the superimposed lattices are expected to give rise to moiré fringes of the translational type, since the two relevant lattice parameters are different. Considering that a fringe moiré pattern is produced by a single set of parallel overlapping lattice planes of the AlN/Al_2O_3 system, in (0001) orientation where three sets of equivalent planes are present, three intersecting equidistant fringe moiré patterns will appear, resulting in the formation of a two-dimensional translational moiré pattern. Moreover, every individual moiré pattern of the complex pattern will be rotated with respect to the other by 60°, since moiré fringes are perpendicular to the $\mathbf{\Delta g}$ vector producing the pattern and, thus, parallel to the corresponding crystal planes.

A low-magnification plan-view HREM image of the AlN/Al_2O_3 system is illustrated in Fig. 1(a), depicting the formation of a two-dimensional translational moiré pattern, when the electron beam is oriented parallel to the (0001) crystallographic axes of the two overlapping lattices. The coalescence of adjacent AlN islands during the initial stages of the epilayer growth on the substrate is also observed. Taking into account that one doubly diffracted beam with the undiffracted beam contributes in order to produce a fringe moiré pattern, here the combination of three doubly diffracted beams with the transmitted beam produces the complex image of Fig. 1(a). This is soundly demonstrated in the corresponding common diffraction pattern of Fig. 1(b), where satellite spots appear around the basic reflections of the two crystals due to double diffraction. In Fig. 2, two fringe moiré patterns of the AlN/Al_2O_3 system are shown, produced by two different sets of $10\bar{1}0$ AlN/$11\bar{2}0$ Al_2O_3 reflections, in two-beam conditions. The average experimental moiré spacing D_{expt}, measured from over 150 fringes, is found to be $D_{expt}=2.16$ nm and corresponds to one moiré fringe every 8 atomic planes of AlN or 9 atomic planes of Al_2O_3, respectively. It has to be noted that in certain areas of the interface moiré fringes are either more closely or more widely spaced, corresponding to one moiré fringe every 6–7 atomic planes of AlN for the first case and 9–10 atomic

planes of AlN for the second case. Since moiré patterns are sensitive to local distortions, other interfacial features are also revealed from these images. For instance, the occurrence of threading dislocations is readily deduced from the terminating moiré fringes that are shown inside solid white circles of Fig. 2. Dislocation density measurements from various areas of the moiré patterns showed an average density of dislocations of the order of 1.5×10^{11} cm^{-2}. Near the surface of the GaN overgrowth, threading dislocation densities of the order of 8×10^{10} cm^{-2} have been measured, which are in agreement with those reported to occur in GaN films grown on sapphire by different deposition techniques.[3,5] Therefore, it appears that threading dislocations existing in GaN films are related to the interfacial dislocations, also indicated by the connection of threading dislocation lines with terminating moiré fringes at the level of the buffer/substrate interface. Discontinuous shifts along line moiré patterns are also observed in the TEM micrograph of Fig. 2, suggesting the presence of stacking faults (SF's).[4,6] These can be either SF's in prismatic orientation or basal SF's, since the displacement field of the partial dislocations associated with them would produce a displacement of the moiré fringes. Traces connecting shifted moiré fringes are usually parallel to the $\{11\bar{2}0\}$ planes of AlN, indicating that SF's along prismatic planes, emanating from the AlN/Al_2O_3 interface, are dominant. The discontinuous shifts along moiré patterns are viewed in the dashed white ellipses of Fig. 2.

The indirect evidence of the existence of threading dislocations by terminating moiré fringes is confirmed in the plan-view HREM images of Fig. 3 viewed along $[0001]$ axes of the two lattices. Figure 3(a) shows three sets of moiré fringes that reveal the hexagonal symmetry of the (0001) interface. In this micrograph the structure of the epitaxial interface is shown, since the three sets of $\{10\bar{1}0\}$ lattice planes of AlN and $\{11\bar{2}0\}$ lattice planes of Al_2O_3 that overlap are resolved. Such moiré patterns, which are a magnified view of the crystal structure, could be used to locate the edge component of threading dislocations emerging from the epitaxial interface. The white arrows depict two terminating moiré fringes indicating the position of a threading dislocation. The black arrows are placed on the projection of two extra prismatic half-planes, which are associated with this threading dislocation. A schematic illustration of the above-mentioned misfit dislocation network is shown in Fig. 3(b), given in the same orientation with Fig. 3(a). The two thick solid lines depict the misfit dislocations arising from two missing AlN half-planes, the other parts of which are associated with the threading dislocation. A magnified region of Fig. 3(a) that contains the threading dislocation is shown in Fig. 3(c), which is Fourier filtered in order to reveal solely the AlN structure. The extra half-planes of the threading dislocation coincide with the black arrows pointing towards the core of the dislocation.[7–9] The Burgers circuit drawn around the dislocation determines the edge component of the Burgers vector, that is, $\mathbf{b}_\perp = 1/3\langle 11\bar{2}0\rangle$. This suggests that the threading dislocation is either of a pure edge character ($\mathbf{b}=\mathbf{a}$) or of a mixed character ($\mathbf{b}=\mathbf{a}+\mathbf{c}$). However, determination of the Burgers vector inside the GaN film showed that, in our case, the vast majority of threading dislocations are of the **a** type. It is worth noting that the strong white contrast pointed out by the white arrows in Fig. 3(a) is actually a magnified image of the dislocation core. In addition, the existence of the extra half-planes in the lattice with the larger parameter (AlN) causes a reversal of the sense of the dislocation image in the moiré patterns [Fig. 3(a)].[4]

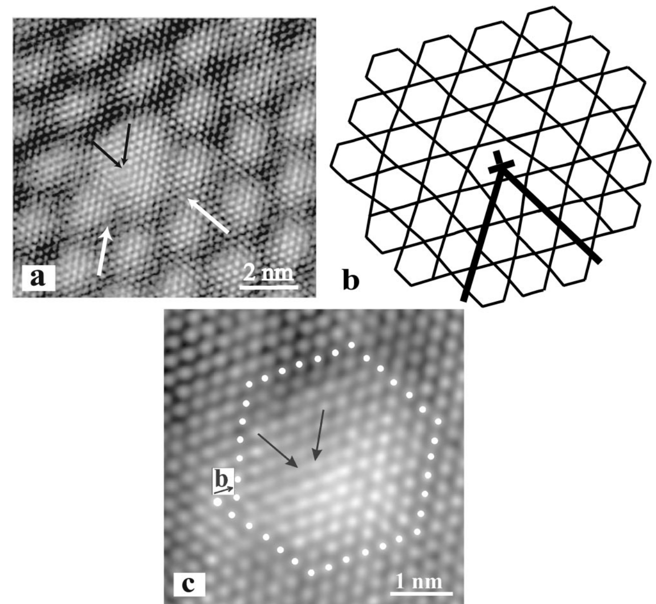

FIG. 3. (a) Plan-view HREM image, viewed along $[0001]$ axes of the two lattices, illustrating three sets of moiré fringes and the structure of the epitaxial interface. The white arrows depict two terminating moiré fringes indicating the position of a threading dislocation. The black arrows are placed on the projection of two extra prismatic half-planes, which are associated with this threading dislocation. (b) Schematic illustration of the misfit dislocation network shown in (a). The two thick lines depict the misfit dislocations arising from two missing AlN half-planes, the other parts of which are associated with the threading dislocation. (c) Fourier filtered image of a magnified area of (a), containing the threading dislocation, which reveals only the AlN structure. The extra half-planes coincide with the black arrows pointing towards the core of the threading dislocation, while the Burgers circuit drawn around determines the edge component of the Burgers vector that is $1/3\langle 11\bar{2}0\rangle$.

IV. DISCUSSION

The spacing of the moiré fringes is given by

$$D=\frac{d_e d_s}{d_e-d_s}, \tag{1}$$

where d_e and d_s are the corresponding d spacings of the overlapping planes of the epilayer and the substrate, respectively.[3,4] Applying Eq. (1) for $d_e(10\bar{1}0$ AlN$)=0.2695$ nm and $d_s(11\bar{2}0$ $Al_2O_3)=0.2379$ nm, we find $D=2.029$ nm, which corresponds to one moiré fringe every 7.5 atomic planes AlN or 8.5 atomic planes of Al_2O_3. Consequently, in a stress-free configuration, moiré fringes are expected to appear in a successive variation of 7–8 atomic planes of AlN or 8–9 atomic planes of Al_2O_3, which differs

from the majority of the experimental observations ($D_{expt}=2.16$ nm). The natural or lattice misfit m between the two crystal lattices, taking AlN as the reference crystal, is given by the known expression[4,10–12]

$$m=\frac{d_s-d_e}{d_e}, \quad (2)$$

which, in this case, results in $m=-0.1173$ or -11.73%. Thus, a compressive strain is exerted on the thin AlN epilayer, whereas the substrate due to its large thickness is considered to be unaffected and its lattice parameters to be constant. Since the thickness of the epilayer is large enough (100 nm), the mismatch between the two crystals could be relaxed by a network of misfit dislocations introduced in the plane of the interface. The effective misfit δ in a relaxed configuration is given by[3,4,12]

$$\delta=\frac{d_s-d_e^{ef}}{d_e}, \quad (3)$$

where d_e^{ef} is the average experimental d spacing of the epilayer planes measured after relaxation. Using the experimental moiré spacing D_{expt}, we find from Eq. (1) that $d_e^{ef}=0.2673$ nm, which was expected due to compression of the epilayer parameter. Thus, Eq. (3) results in $\delta=-0.1091$ meaning that 93% of the compressive strain on the AlN epilayer is relaxed through the introduction of the misfit dislocation network. Since δ has a smaller absolute value than m, a negative (compressive) residual strain e_r, which reduces further the natural difference of the lattice parameters between the substrate and the epilayer, has to be taken into account. Therefore, the lattice misfit can be written as

$$m=\delta+e_r. \quad (4)$$

Since both crystals belong to the hexagonal crystal system, the misfit dislocation network consists of three equivalent sets of perfect 60° dislocations. The Burgers vector of the misfit dislocations corresponds to $\mathbf{b}=1/3\langle 11\bar{2}0\rangle$ in terms of the AlN lattice or $\mathbf{b}=1/3\langle 10\bar{1}0\rangle$ in terms of the Al_2O_3 lattice. The spacing between edge misfit dislocations is given by[4]

$$D_d=\frac{|\mathbf{b}|}{\delta}. \quad (5)$$

Estimating the dislocation spacing in terms of the d spacing of $\{11\bar{2}0\}$ planes of Al_2O_3 that remains unaffected, for 60° dislocations instead of $|\mathbf{b}|$ we should use $|\mathbf{b}|\cos 30°$, which is the edge component of $\mathbf{b}$ along the corresponding $\langle 11\bar{2}0\rangle$ direction in the Al_2O_3 lattice. Taking this into account and applying Eq. (5) for $\mathbf{b}=a\sqrt{3}=0.2747$ nm, the dislocation spacing is found to be $D_d=2.18$ nm, which is practically equal to the average moiré spacing. Additionally, the operating reciprocal lattice vectors $\mathbf{g}$ of the $\{10\bar{1}0\}$ AlN/$\{11\bar{2}0\}$ Al_2O_3 lattice planes are perpendicular to the direction of the dislocation lines and thus, in our case, the images of the hexagonal moiré pattern and the misfit dislocation network should be identical.[4] Under the two-beam dynamical diffracting conditions of Fig. 2 two sets of misfit dislocations should be visible, the third being in extinction due to the satisfaction of the $\mathbf{g}\cdot\mathbf{b}=0$ criterion. However, the one set overlaps with the moiré fringes and the second set presents no contrast at all. This can be explained considering that the distance between dislocations of the periodic arrays (2.18 nm) is of the order of the core diameter of the dislocations, assuming a core radius of approximately 1 nm.[13] Thus, the strain fields of neighboring dislocations are in close vicinity and do not produce a significant variation of contrast in conventional TEM observations.

An edge threading dislocation with a line direction along the c axis is related to two extra $\{10\bar{1}0\}$ half-planes,[1,7,8] as is shown in Figs. 3(a) and 3(c). The corresponding missing half-planes are associated with two misfit dislocations at the interfacial dislocation network in the way that is shown in Fig. 3(b). The Burgers vector of the threading dislocation is equal to the algebraic sum of the Burgers vectors of the two misfit dislocations that are associated with it, in order to conserve Frank's rule of dislocation nodes. Thus, in hexagonal systems, threading dislocations associated with misfit dislocations possess an **a** type Burgers vector lying in the interface. The link between the two defects allows us to assume that a threading dislocation may be formed by interfacial misfit dislocations. Since there is no shear stress acting on the threading dislocations,[14] their occurrence can be attributed to the coalescence of adjacent misoriented islands at the early stages of AlN growth.[15,16] The observed, in the GaN overgrowth, $\mathbf{a}+\mathbf{c}$ threading dislocations probably result from interactions between **a**-edge dislocations emerging from the interface with **c**-screw dislocations existing in the film.[17,18]

The analysis of moiré patterns indirectly demonstrated that, in most cases, a misfit dislocation should be introduced every 8 atomic planes of AlN or 9 atomic planes of Al_2O_3. This is clearly verified in the cross-section HREM image of Fig. 4(a), where the AlN/Al_2O_3 interface is depicted, viewed along the $\langle 11\bar{2}0\rangle$ AlN/$\langle 10\bar{1}0\rangle$ Al_2O_3 axes. Using Fourier filtering, it is possible to visualize the edge component of one set of misfit dislocations as terminating fringes of the corresponding substrate lattice planes.[3,19] Figure 4(b) shows a filtered image using the in-plane Fourier spatial frequencies, where $\{11\bar{2}0\}$ Al_2O_3 lattice fringes terminate at the interface in nine fringe intervals. In plan-view geometry, the position of the misfit dislocations is localized in regions of bad fit between the two crystals. That is clearly identified in the plan-view HREM image of Fig. 5(a), where sharp contrast projected atomic columns indicate regions of good fit, while blurred contrast projected atomic columns indicate regions of bad fit. In addition, applying a Fourier transform to the HREM image of Fig. 5(a) and using only one set of parallel Fourier spatial frequencies ($10\bar{1}0$ AlN/$11\bar{2}0$ Al_2O_3) we obtain filtered images of one set of $\{10\bar{1}0\}$ AlN lattice fringes and the corresponding parallel set of $\{11\bar{2}0\}$ Al_2O_3 lattice fringes. Figure 5(b) is a superposition of the two separate Fourier filtered images which reveals the areas where

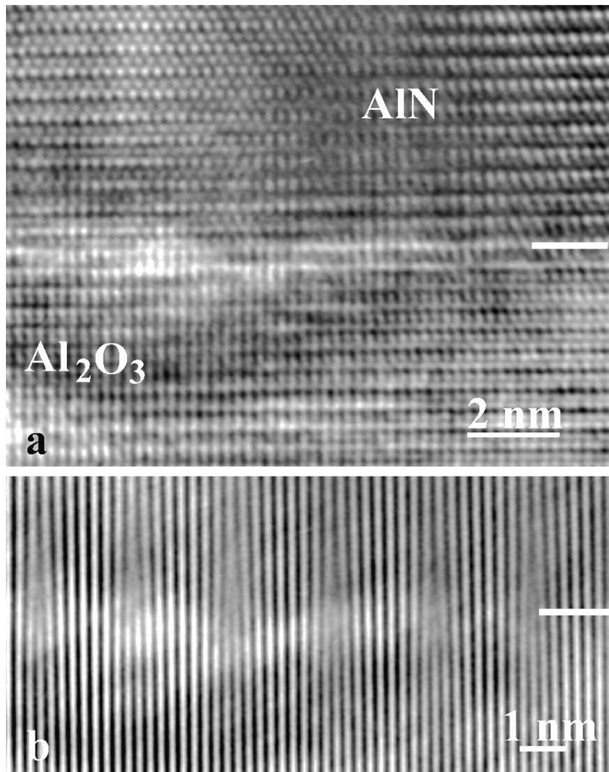

FIG. 4. (a) Cross-section HREM image, viewed along the $\langle 11\bar{2}0\rangle$ AlN/$\langle 10\bar{1}0\rangle$ Al_2O_3 axes, where the AlN/Al_2O_3 interface is illustrated. (b) Fourier filtered image taken from (a), using the in-plane Fourier spatial frequencies, where $\{11\bar{2}0\}$ Al_2O_3 lattice fringes are shown to terminate at the interface in nine fringe intervals. White solid lines in (a) and (b) denote the position of the interface plane.

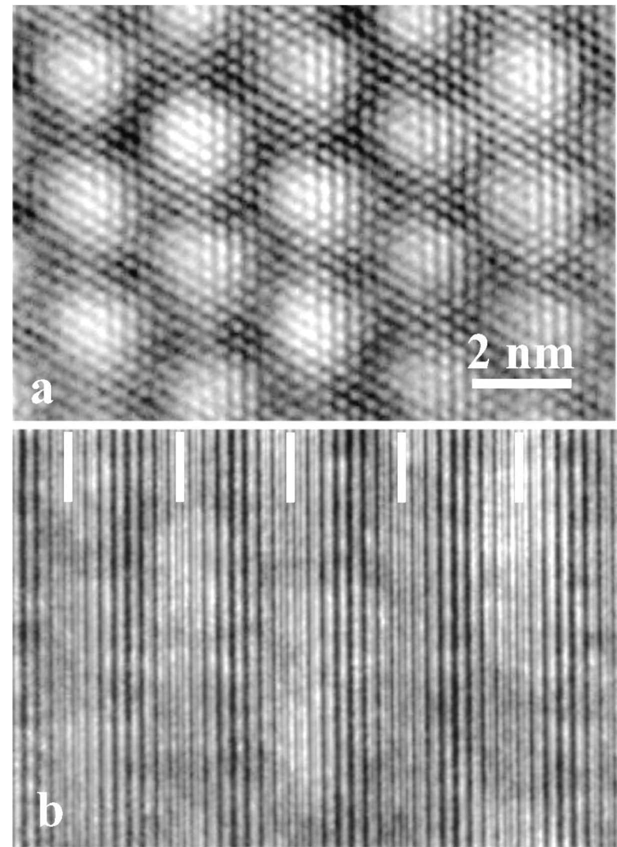

FIG. 5. (a) Plan-view HREM image, viewed along [0001] axes of the two lattices, where regions of good and bad fits are indicated by sharp and blurred contrast projected atomic columns, respectively. (b) HREM image synthesized from the superposition of two separate Fourier filtered images of (a), revealing the areas where parallel planes of the two crystals ($\{10\bar{1}0\}$ AlN//$\{11\bar{2}0\}$ Al_2O_3) are in good and bad fits. White solid lines in areas of bad fit indicate the location of misfit dislocations.

parallel planes of the two crystals are in good and bad fits. White solid lines in areas of bad fit denote the position of misfit dislocations.

Due to the difference between effective and natural misfit in the system, the AlN buffer layer is under a residual elastic strain which is deduced from Eq. (4) to be $e_r = -8.2 \times 10^{-3}$ or -0.82%. Using this value in Eq. (5), we found that the relaxation of residual strain would require the insertion of an additional misfit dislocation network with a spacing of 29 nm. This corresponds to one additional misfit dislocation every 109 $\{10\bar{1}0\}$ lattice planes of AlN or equivalently 122 $\{11\bar{2}0\}$ lattice planes of Al_2O_3. In terms of moiré patterns, this would correspond, roughly, to one additional moiré fringe every 13 fringes, taking into account that the experimental moiré fringe spacing is 2.16 nm. Measurements on the TEM micrographs of Fig. 2 showed that, at various areas of the interface, an additional moiré fringe is introduced every 11–17 fringes, which could account for a local relaxation of the residual strain. In addition, it has been argued that the in-plane component of basal SF's can compensate a part of the residual strain.[20] This can be expanded to include also SF's in prismatic orientation, since the displacement field of their in-plane component could account for a partial relaxation of the residual strain.

V. CONCLUSION

The interfacial misfit in the AlN/Al_2O_3 heterostructure is partially relaxed by a network of three sets of 60° misfit dislocations. Misfit dislocations are usually introduced in regular intervals of 8 atomic planes in terms of the AlN lattice or 9 atomic planes in terms of the Al_2O_3 lattice. This is estimated from the experimental spacing of the moiré fringes and directly verified by cross-section HREM images. Terminating moiré fringes and dislocation density measurements suggest the association of misfit and threading dislocations at the buffer/substrate interface. Plan-view HREM images show that a threading dislocation is directly associated with two extra prismatic AlN half-planes, the missing parts of which are related to misfit dislocations in the interfacial network. The sum of the Burgers vectors of the two misfit dislocations equals the Burgers vector of the associated threading dislocation and thus is of the **a** type. The construction of a Burgers circuit around the core of a threading dislocation observed in plan-view HREM images verified an **a**-type Burgers vector. The observed misfit dislocation network accommodates 93% of the natural compressive misfit (-0.1173) between the two stress-free crystal lattices. The compressive

residual strain retains the AlN buffer layer elastically strained. Using plan-view HREM images, the locations of misfit dislocation at regions of bad fit between the two crystal structures are illustrated.

ACKNOWLEDGMENTS

This work is supported by the EU Project No. HPRN-CT-1999-00040.

*Corresponding author. Electronic address: komnhnoy@auth.gr

[1] R. Jones, Mater. Sci. Eng., B **71**, 24 (2000).

[2] P. B. Hirsch, in *Polycrystalline Semiconductors II*, Springer Proceedings in Physics, Vol. 54, edited by J. H. Werner and H. P. Strunk (Springer-Verlag, Berlin, 1991).

[3] S. Kaiser, H. Preis, W. Gebhardt, O. Ambacher, H. Angerer, M. Stutzmann, A. Rosenauer, and D. Gerthsen, Jpn. J. Appl. Phys., Part 1 **37**, 84 (1998).

[4] P. B. Hirsch, A. Howie, R. B. Nicholson, D. W. Pashley, and M. J. Whelan, *Electron Microscopy of Thin Crystals* (Butterworths, London, 1965), pp. 343–378.

[5] X.H. Wu, P. Fini, E.J. Tarsa, B. Heying, S. Keller, U.K. Mishra, S.P. DenBaars, and J.S. Speck, J. Cryst. Growth **189/190**, 231 (1998).

[6] M. J. Stowell, in *Epitaxial Growth*, edited by J. W. Matthews (Academic, New York, 1975), Pt. B.

[7] Y. Hin, S.J. Pennycook, N.D. Browning, P.D. Nellist, S. Sivananthan, F. Omnes, B. Baumont, J.P. Faurie, and P. Gibart, Appl. Phys. Lett. **72**, 2680 (1998).

[8] J. Kang and T. Ogawa, J. Cryst. Growth **210**, 157 (2000).

[9] P. Ruterana, V. Potin, G. Nouet, R. Bonnet, and M. Loubradou, Mater. Sci. Eng., B **59**, 177 (1999).

[10] J. H. Van Der Merwe and C. A. B. Ball, in *Epitaxial Growth*, edited by J. W. Matthews (Academic, New York, 1975), Pt. B.

[11] J. W. Matthews, in *Epitaxial Growth*, edited by J. W. Matthews (Academic, New York, 1975), Pt. B.

[12] R. Scholtz and J. Woltersdorf, in *Electron Microscopy in Solid State Physics*, edited by H. Bethge and J. Heydenreich (Elsevier, Amsterdam, 1987).

[13] D. Hull and D. J. Bacon, *Introduction to Dislocations* (Pergamon, Oxford, 1984), p. 77.

[14] X.J. Ning, F.R. Chien, P. Pirouz, J.W. Yang, and M. Ashif Khan, J. Mater. Res. **11**, 580 (1996).

[15] H.P. Strunk, M. Albrecht, S. Christiansen, W. Dorsch, U. Hörmann, B. Jahnen, and T. Remmele, Phys. Status Solidi A **171**, 215 (1999).

[16] D.J. Dunstan, J. Mater. Sci.: Mater. Electron. **8**, 337 (1997).

[17] D. Cherns, W.T. Young, and F.A. Ponce, Mater. Sci. Eng., B **50**, 76 (1997).

[18] X.H. Wu, L.M. Brown, D. Kapolnek, S. Keller, B. Keller, S.P. DenBaars, and J.S. Speck, J. Appl. Phys. **80**, 3228 (1996).

[19] P. Ruterana, V. Potin, B. Barbaray, and G. Nouet, Philos. Mag. A **80**, 937 (2000).

[20] P. Vennegues, B. Beaumont, M. Vaille, and P. Gibart, J. Cryst. Growth **173**, 249 (1997).